# The $^{93}$Zr$(n,\gamma)$ reaction up to 8 keV neutron energy

G. Tagliente,[1,*] P. M. Milazzo,[2] K. Fujii,[2] U. Abbondanno,[2] G. Aerts,[3] H. Álvarez,[4] F. Alvarez-Velarde,[5] S. Andriamonje,[3] J. Andrzejewski,[6] L. Audouin,[7] G. Badurek,[8] P. Baumann,[9] F. Bečvář,[10] F. Belloni,[2] E. Berthoumieux,[3] F. Calviño,[11] M. Calviani,[12] D. Cano-Ott,[5] R. Capote,[13,14] C. Carrapiço,[15] P. Cennini,[16] V. Chepel,[17] E. Chiaveri,[16] N. Colonna,[1] G. Cortes,[11] A. Couture,[18] M. Dahlfors,[16] S. David,[9] I. Dillmann,[7,19] C. Domingo-Pardo,[20,19] W. Dridi,[3] I. Duran,[4] C. Eleftheriadis,[21] M. Embid-Segura,[5] A. Ferrari,[16] R. Ferreira-Marques,[17] W. Furman,[22] I. Goncalves,[15] E. Gonzalez-Romero,[5] F. Gramegna,[12] C. Guerrero,[5] F. Gunsing,[3] B. Haas,[23] R. Haight,[24] M. Heil,[7,19] A. Herrera-Martinez,[16] E. Jericha,[8] F. Käppeler,[7] Y. Kadi,[16] D. Karadimos,[25] D. Karamanis,[25] M. Kerveno,[9] E. Kossionides,[26] M. Krtička,[10] C. Lamboudis,[21] H. Leeb,[8] A. Lindote,[17] I. Lopes,[17] S. Lukic,[9] J. Marganiec,[6,19] S. Marrone,[1] T. Martínez,[5] C. Massimi,[27] P. Mastinu,[12] A. Mengoni,[13] C. Moreau,[2] M. Mosconi,[7,28] F. Neves,[17] H. Oberhummer,[8] S. O'Brien,[18] C. Papachristodoulou,[25] C. Papadopoulos,[29] C. Paradela,[4] N. Patronis,[25] A. Pavlik,[30] P. Pavlopoulos,[31] L. Perrot,[3] M. T. Pigni,[8] R. Plag,[7,19] A. Plompen,[32] A. Plukis,[3] A. Poch,[11] J. Praena,[12] C. Pretel,[11] J. Quesada,[14] R. Reifarth,[24,19] M. Rosetti,[33] C. Rubbia,[34] G. Rudolf,[9] P. Rullhusen,[32] J. Salgado,[15] C. Santos,[15] L. Sarchiapone,[16] I. Savvidis,[21] C. Stephan,[35] J. L. Tain,[20] L. Tassan-Got,[35] L. Tavora,[15] R. Terlizzi,[1] G. Vannini,[27] P. Vaz,[15] A. Ventura,[33] D. Villamarin,[5] M. C. Vincente,[5] V. Vlachoudis,[16] R. Vlastou,[29] F. Voss,[7] S. Walter,[7] M. Wiescher,[18] and K. Wisshak[7]

(n_TOF Collaboration[†])

[1]*Istituto Nazionale di Fisica Nucleare (INFN), Bari, Italy*
[2]*Istituto Nazionale di Fisica Nucleare (INFN), Trieste, Italy*
[3]*CEA, Irfu, Gif-sur-Yvette, France*
[4]*Universidade de Santiago de Compostela, Spain*
[5]*Centro de Investigaciones Energeticas Medioambientales y Technologicas, Madrid, Spain*
[6]*University of Lodz, Lodz, Poland*
[7]*Karlsruhe Institute of Technology (KIT), Campus Nord, Institut für Kernphysik, Karlsruhe, Germany*
[8]*Atominstitut der Österreichischen Universitäten,Technische Universität Wien, Austria*
[9]*Centre National de la Recherche Scientifique/IN2P3 - IReS, Strasbourg, France*
[10]*Faculty of Mathematics and Physics, Charles University in Prague, Czech Republic*
[11]*Universitat Politecnica de Catalunya, Barcelona, Spain*
[12]*Istituto Nazionale di Fisica Nucleare (INFN), Laboratori Nazionali di Legnaro, Italy*
[13]*International Atomic Energy Agency (IAEA), NAPC/Nuclear Data Section, Vienna, Austria*
[14]*Universidad de Sevilla, Spain*
[15]*Instituto Tecnológico e Nuclear (ITN), Lisbon, Portugal*
[16]*CERN, Geneva, Switzerland*
[17]*LIP - Coimbra & Departamento de Fisica da Universidade de Coimbra, Portugal*
[18]*University of Notre Dame, Notre Dame, USA*
[19]*GSI Darmstadt, Darmstadt, Germany*
[20]*Instituto de Física Corpuscular, CSIC-Universidad de Valencia, Spain*
[21]*Aristotle University of Thessaloniki, Greece*
[22]*Joint Institute for Nuclear Research, Frank Laboratory of Neutron Physics, Dubna, Russia*
[23]*Centre National de la Recherche Scientifique/IN2P3 - CENBG, Bordeaux, France*
[24]*Los Alamos National Laboratory, New Mexico, USA*
[25]*University of Ioannina, Greece*
[26]*NCSR, Athens, Greece*
[27]*Dipartimento di Fisica, Università di Bologna, and Sezione INFN di Bologna, Italy*
[28]*PTB Braunschweig, Braunschweig, Germany*
[29]*National Technical University of Athens, Greece*
[30]*University of Vienna, Faculty of Physics, Vienna, Austria*
[31]*Pôle Universitaire Léonard de Vinci, Paris La Défense, France*
[32]*CEC-JRC-IRMM, Geel, Belgium*
[33]*ENEA, Bologna, Italy*
[34]*Università degli Studi di Pavia, Pavia, Italy*
[35]*Centre National de la Recherche Scientifique/IN2P3 - IPN, Orsay, France*

(Received 31 July 2012; revised manuscript received 11 December 2012; published 31 January 2013)

The $(n,\gamma)$ reaction of the radioactive isotope $^{93}$Zr has been measured at the n_TOF high-resolution time-of-flight facility at CERN. Resonance parameters have been extracted in the neutron energy range up to 8 keV,

 

yielding capture widths smaller (14%) than reported in an earlier experiment. These results are important for detailed nucleosynthesis calculations and for refined studies of waste transmutation concepts.

DOI: 10.1103/PhysRevC.87.014622 PACS number(s): 25.40.Lw, 25.70.Ef, 27.60.+j, 28.41.Qb

## I. INTRODUCTION

The elements heavier than iron are produced via neutron capture reactions in the slow ($s$) and rapid ($r$) neutron capture processes, except for a minor contribution from the so-called $p$-process [1–3]. The $s$-process occurs at temperatures of $\approx$1–10 $\times$ $10^8$ K and corresponding neutron densities of $\approx 10^6$–$10^{12}$ cm$^{-3}$, where the time between neutron capture events is of the order of years, much slower than the average $\beta$-decay times. The $r$-process, which is associated with explosive nucleosynthesis in supernovae and/or neutron star mergers, is characterized by high temperatures of about 2–3 $\times$ $10^9$ K and neutron densities well above $10^{20}$ cm$^{-3}$, resulting in neutron capture times of the order of milliseconds. The stellar sites of the $s$-process are thermally pulsing low-mass asymptotic giant branch (AGB) stars, which contribute to the main $s$ component from Zr to Pb/Bi [4] and the core He and shell C burning phases in massive stars, which are producing the weak $s$ component between Fe and Zr [5].

Because of the slow time scale for neutron capture, the reaction path of the $s$-process follows the valley of $\beta$ stability. On that path the Zr isotopes occupy the particularly interesting region just at the border between the weak and main component. The stable isotopes $^{90,91,92,94}$Zr are predominantly of $s$-process origin because they exhibit rather small $(n,\gamma)$ cross sections as a consequence of their vicinity to the magic neutron number $N = 50$.

The radioactive isotope $^{93}$Zr can be considered as stable on the time scale of the $s$-process because of its long half-life of 1.6 Myr. The corresponding $s$ abundance of $^{93}$Zr decays only later to provide the $s$ component of the daughter $^{93}$Nb, which itself is bypassed by the direct $s$-process reaction chain.

While the isotopic ratios of most elements can only be inferred from terrestrial material, which represents an average of many sources, Zr isotope ratios can also be determined for single sources, either by analyses of microscopic dust grains of presolar origin or by spectroscopy of the band structure of ZrO in cool AGB stars.

Presolar grains can be recovered from primitive meteorites [6]. Laboratory analyses of these $\mu$m-sized grains have revealed isotopic patterns completely different from those of the bulk of solar system material [7]. Since isotopic compositions can only be modified by nuclear reactions, stardust grains carry the signature of their formation environments around different types of astrophysical objects, from giant stars to novae and supernovae.

Among the variety of presolar dust grains, the best studied species are silicon carbide (SiC) grains, which are considered to originate from the envelopes of carbon-rich low-mass AGB stars. Because they occur in relatively large sizes, even the isotopic composition of trace elements can be determined. In fact the Zr and Nb abundance patterns are used to infer constraints for the $s$-process neutron density in the individual stars [8,9]. In this context, the $^{93}$Zr$(n,\gamma)$ cross section needs to be known with an accuracy of 3–5%.

Zirconium isotopic abundances can even be spectroscopically observed in cool stars via the ZrO bandheads near 6925 Å (see for example Ref. [10]). The observed $s$-process patterns were found in fair agreement with stellar model predictions, which, however, depend on the neutron capture cross sections of the involved isotopes.

The $(n,\gamma)$ cross section of $^{93}$Zr is also of great interest for technological reasons, because Zr alloys are largely used as structural material in nuclear reactors and because $^{93}$Zr is one of the major long-lived fission products. Therefore, transmutation via neutron capture is given high priority to reduce the long-term hazards. One possibility is irradiation using a fusion driven neutron source with high-flux blanket that has been shown to transmute $^{93}$Zr sufficiently, thus resolving the problem of its accumulation within the time period of several decades [11].

So far, experimental data for the $^{93}$Zr cross section are very scarce. In a time-of flight (TOF) experiment performed at the Oak Ridge Linear Accelerator [12], resonances have been identified up to 21.5 keV neutron energy. The only other available measurement reports information on the thermal capture cross section [13].

The measurement of the $^{93}$Zr $(n,\gamma)$ cross section is essentially hampered by its smallness as well as by the radioactivity and the low enrichment of the sample, where the last point is particularly crucial. The presently available ZrO sample, which has already been used in the previous TOF measurement [12], was isolated from fission products and contains, therefore, all stable isotopes as well. The limited enrichment in $^{93}$Zr of $\approx$20% implies that substantial corrections of the measured yield were required. The corresponding uncertainties could only be avoided for well-separated resonances, thus calling for a high-resolution TOF measurement.

In view of this situation the $^{93}$Zr$(n,\gamma)$ cross section has been measured up to 8 keV neutron energy using the unique features of the n_TOF facility at CERN, which combines excellent resolution, high instantaneous neutron flux and low background [14]. Details of the measurement are described in Sec. II, resonance analyses and results are presented in Sec. III, and their effect on the Maxwellian-averaged capture cross sections is discussed in Sec. IV.

## II. MEASUREMENT

The measurement was performed at the CERN n_TOF facility [14,15], where neutrons are produced by spallation reactions of a 20 GeV/$c$ pulsed proton beam hitting a massive lead block. With a conversion ratio of 300 neutrons per proton, each beam pulse of 7 $\times$ $10^{12}$ protons produces a neutron flux

*Corresponding author: giuseppe.tagliente@ba.infn.it
†www.cern.ch/ntof

of $10^5$ neutrons/cm$^2$/pulse at the sample position, 187.5 m from the spallation target. The fast spallation neutrons are moderated in the 5.8 cm thick layer of cooling water around the lead target, resulting in a wide neutron spectrum from thermal up to 1 GeV. Thanks to the long flight path and to the short pulse width of 6 ns, the resolution in neutron energy is better than 0.1% in the range of the present measurement, i.e., below 8 keV.

The lead spallation target is connected with the experimental area by an evacuated beam line. Charged particles are removed from the neutron beam by a 1.5 T sweeping magnet, and neutrons and ultrarelativistic particles outside the beam line are suppressed by heavy concrete walls and a massive iron shielding 3.5 m in thickness. The neutron beam is shaped by two collimators, the second one placed close to the last shielding wall upstream of the experimental area. The 18 mm aperture of the second collimator gives rise to a nearly symmetric Gaussian-shaped beam profile at the sample position. The beam line extends 12 m beyond the experimental area to minimize the effect of back-scattered neutrons.

The neutron flux was determined relative to the $^{235}$U$(n,f)$ cross section by means of a calibrated fission chamber from PTB Braunschweig [14]. During the measurement the flux was checked online by a low-mass $^6$Li neutron monitor [16].

The measurement was carried out by detection of the prompt $\gamma$-ray cascade following neutron capture. Two $\gamma$-detectors consisting of $C_6D_6$ liquid scintillator cells were placed perpendicular to the neutron beam at a distance of about 3 cm from the beam axis and 9.2 cm backward from the sample position. In view of the large scattering/capture cross section ratio of $^{93}$Zr, special care was taken to reduce the neutron sensitivity of the experimental setup to the smallest possible level. This was achieved by minimizing the mass of the setup and of the scintillator cells and by using only materials with very low $(n,\gamma)$ cross sections (such as C, O, and Si) for the construction [17]. The scintillator cells were directly coupled to EMI-9823QKB photomultiplier tubes. The light output of the detectors was calibrated at 662, 1173, and 1332 keV by means of $^{137}$Cs and $^{60}$Co reference sources. An additional calibration point at 6.13 MeV was obtained by means of a composite $^{238}$Pu/$^{13}$C source. The calibration was repeated in regular intervals to verify the stability of the detectors. The detector signals were recorded using the standard n_TOF data acquisition system based on fast digitizers with a sampling rate of 500 Msamples/s [18].

The sample was prepared starting from the $ZrO_2$ powder already used in Ref. [12]. It was pressed to a pellet 22 mm in diameter, 3.5 mm in thickness, and 4.46 g in mass, which was then encapsulated twice using an inner Al and a welded outer Ti container, both with 0.2 mm thick walls. The $^{93}$Zr activity was 62.6 MBq. The isotopic composition of the sample was adopted from Ref. [12] (Table I). The sample contained also traces of Mo and Sn. Although these impurities were below 0.01%, their contribution to the measured capture yield was not negligible and had to be considered in data analysis. Additional Au and Pb samples of the same diameter were used for repeated neutron flux measurements and background runs throughout the experiment.

TABLE I. Isotopic composition of the sample (in atomic %).

| $^{90}$Zr | $^{91}$Zr | $^{92}$Zr | $^{93}$Zr | $^{94}$Zr | $^{96}$Zr |
|---|---|---|---|---|---|
| 2.29 | 18.61 | 18.95 | 19.98 | 20.50 | 19.67 |

## III. DATA ANALYSIS AND RESULTS

Neutron capture events were identified by the prompt $\gamma$-ray cascade emitted from the compound nucleus. Given that the corresponding $\gamma$-ray spectrum depends on the sample under study, the intrinsic efficiency of $C_6D_6$ detectors has to be modified by the pulse height weighting technique (PHWT) [19,20]. This technique is based on a software correction of the detector response to obtain a $\gamma$ efficiency linearly proportional to the $\gamma$-ray energy. In this way, the efficiency for capture events becomes constant and proportional to the $Q$ value of the reaction. It has been demonstrated by a detailed study for the setup used at n_TOF that the possible systematic uncertainties introduced by this data analysis procedure are lower than 2%. A full description of the PHWT used at n_TOF is given in Ref. [21].

Because of the low enrichment, the respective corrections for the stable zirconium isotopes, sample impurities, and the various backgrounds are of primary importance for this measurement. Examples for resonances of impurity isotopes are shown in the upper panel of Fig. 1 and in the bottom panel of Fig. 2. These contributions were carefully identified and taken into account in the analysis. The comparison with resonance parameters from measurements with enriched Zr samples provides a consistency check for the isotopic composition of the sample (see below).

At low neutron energies the main background is due to the sample activity. This contribution has been measured

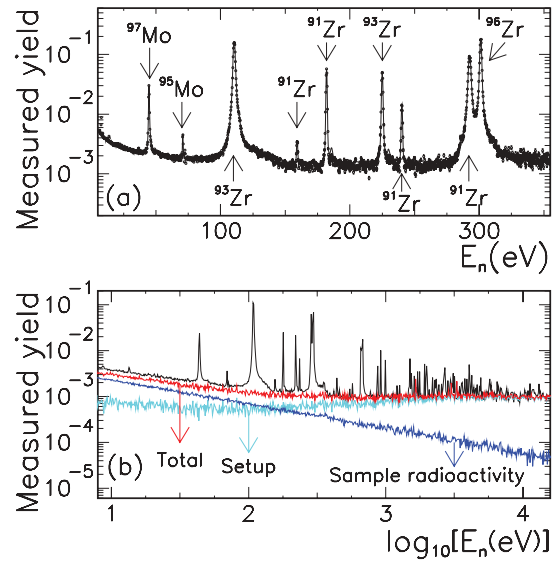


FIG. 1. (Color online) Upper panel: Examples for fits of the measured yield with the $\mathcal{R}$-matrix code SAMMY. Isotopic and elemental impurities in the sample were included in the fit according to their abundances. Lower panel: Measured yield (in black), background due to the radioactivity of the sample (in blue), background due to in-beam $\gamma$ rays and surrounding materials (in turquoise) and the overall background (in red).

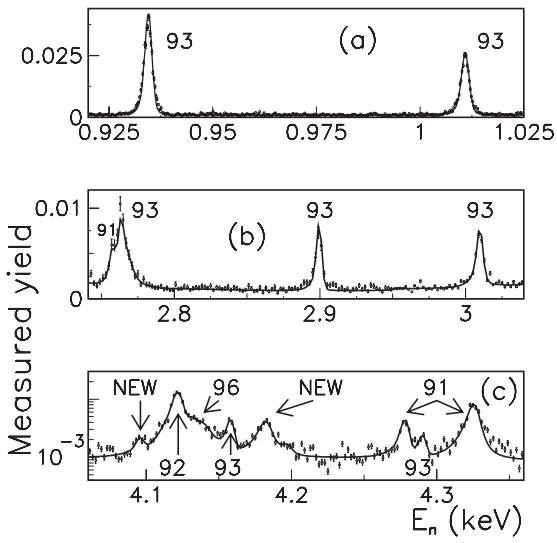


FIG. 2. Examples for fits of the capture yield with the $\mathcal{R}$-matrix code SAMMY. In the data analysis of Ref. [12] resonances coming from other isotopes were subtracted from the measured yield, while in the present analysis it has been preferred to fit all isotopes together. Then, a direct data comparison between present data and those of Ref. [12] is not feasible. (a) Resonances at 934 and 1010 eV. (b) The resonance at 2767 eV was not listed in Ref. [12]; the high resolution of the present measurement allows the discrimination of the resonances at 2.757 and 2.767 keV, which belong to $^{91}$Zr and $^{93}$Zr, respectively. (c) Two new resonances have been assigned to $^{93}$Zr at 4.09 and 4.18 keV. The examples at 4.12 and 4.32 keV, which are listed as $^{93}$Zr resonances in Refs. [12,26], belong to $^{92}$Zr and $^{91}$Zr, respectively.

without neutron beam and was normalized by the acquisition time (blue component in the bottom panel of Fig. 1). Other background components originate from capture of sample scattered neutrons in the detectors or in surrounding materials, from capture events in the aluminum and titanium cans of the sample, from in-beam $\gamma$ rays produced by capture events in the water moderator around the spallation target, and from the ambient background in the experimental area. These backgrounds, which have been discussed in detail elsewhere [22], dominate the overall background for neutron energies above 1 keV. The present resonance analysis was restricted to the region below 8 keV not only for background reasons, but also because the resonances of Ti, one of the $^{93}$Zr sample containers used for security prescriptions, overlap the Zr resonances, not allowing their resolution.

The uncertainty contribution related to the counting statistics is ≈5%. Additional sources of uncertainty are due to the energy dependence of the neutron flux and to the fraction of the neutron beam covered by the sample; these contributions bring an uncertainty of 2%, determined by applying the saturated resonance technique, using a 0.1 mm thick Au sample, to the saturated resonance at 4.9 eV in $^{197}$Au [23].

The capture yield has been investigated by means of an $\mathcal{R}$-matrix analysis, using the SAMMY code in the Reich-Moore approximation [24], to extract individual resonance parameters. The observed resonances were classified according to the composition of the sample, considering the isotopic impurities and the specified contaminants. Corrections for the energy resolution of the neutron beam, for the Doppler broadening of cross-section line shapes, and for self-shielding and neutron multiple scattering were considered. Examples illustrating the quality of the SAMMY fits are shown in Figs. 1 and 2. The deduced resonance energies $E_R$ and capture kernels $K$ are listed in Table II.

The capture kernel of a resonance

$$K = g_s \frac{\Gamma_n \Gamma_\gamma}{(\Gamma_n + \Gamma_\gamma)}$$

is defined by the neutron and capture widths, $\Gamma_n$ and $\Gamma_\gamma$, and the statistical spin factor

$$g_s = \frac{(2J+1)}{(2I_n+1)(2I_{^{93}\mathrm{Zr}}+1)},$$

which is determined by the resonance spin $J$, the spin of the incident neutron $I_n = 1/2$, and the spin of the target nucleus $I_{^{93}\mathrm{Zr}} = 5/2$. The determination of the full set of resonance parameters requires the combination of three measurements: two transmission measurements on samples with different thicknesses (so-called thin and thick [25]) and a capture measurement with a thin sample. The transmission data [12] were never published in the EXFOR library, consequently it is not possible to make a simultaneous analysis with the present capture data; moreover the condition $\Gamma_n \gg \Gamma_\gamma$ or vice versa is not valid for most of the resonances; therefore from present data it is possible to extract information only on the capture kernel, proportional to the capture area.

In total, nine new $^{93}$Zr resonances could be identified in the present analysis. On the other hand, the resonances at 5.879 and 5.950 keV listed in the compilation of Ref. [26] were not confirmed, and four strong resonances quoted in Refs. [12,26] at 4.121, 4.320, 5.914, and 6.641 keV were recognized as belonging to $^{92}$Zr, $^{91}$Zr, $^{27}$Al, and $^{92}$Zr, respectively. On the contrary, the high resolution of the present measurement and those of the stable zirconium isotopes with enriched samples [27–31] has allowed us to recognize that the resonance at 2.767 keV belongs to $^{93}$Zr [in the past analysis [12] it was not possible to resolve this resonance and the $^{91}$Zr one at 2.757 keV; see for instance Fig. 2(b)].

The results have been compared with the extracted resonance parameters of the stable zirconium isotopes with the parameters obtained in previous n_TOF measurements [27–31]. The comparison in Table III shows the very good agreement, thus confirming the isotopic composition of the sample used.

Because the present measurement was restricted to the neutron capture channel, the comparison with the study of Macklin *et al.* [12], which combined capture and transmission measurements, is limited to the capture kernels. On average, our capture kernels are 14% smaller than the results of Ref. [12] as shown in Fig. 3.

Possible reasons for this difference may be found in the more accurate determination of the weighting functions, smaller self-shielding and multiple scattering corrections, and lower backgrounds. Modern data acquisition techniques with fast digitizers allowed us to perform off-line data analyses in the most flexible way, including an efficient pulse shape analysis for $n/\gamma$ discrimination. With respect to the background

TABLE II. Resonance parameters $E_R$ and capture kernels $K$. Parameters for resonances with poor resolution are given between square brackets.

| [a]$E_R$ (eV) | [a]$K$ (meV) |
|---|---|
| 110.383(2) | 37.16(8) |
| 225.035(4) | 6.64(5) |
| 669.096(9) | 25.2(3) |
| 693.27(1) | 50.0(4) |
| 882.11(3) | 3.9(1) |
| 934.34(1) | 43.7(5) |
| 1010.72(1) | 30.5(4) |
| 1237.89(4) | 7.5(2) |
| [n]1497.9(1) | 3.2(6) |
| 1574.72(4) | 28.9(7) |
| 1642.21(4) | 24.(1) |
| 1708.5(1) | 6.4(7) |
| 1743.16(3) | 40(1) |
| 1802.42(3) | 41.4(8) |
| 2053.29(5) | 42(1) |
| 2116.32(8) | 10.9(5) |
| 2209.3(1) | 7.1(5) |
| 2320.18(6) | 44(2) |
| 2358.8(1) | 19(1) |
| 2404.0(1) | 7.0(5) |
| 2610.75(6) | 35(2) |
| [n]2767.4(4) | 94(8) |
| 2898.52(6) | 54(3) |
| 3008.7(1) | 69(2) |
| [n]3162.0(5) | 79(9) |
| 3251.43(7) | 90(2) |
| 3511.4(2) | 48(2) |
| 3690.0(1) | 43(2) |
| 3698.5(2) | 46(2) |
| [n]3872.3(2) | 61(5) |
| 3996.1(2) | 55(3) |
| [n]4093.5(5) | 11(2) |
| 4130(1) | 59(9) |
| 4156.0(2) | 44(4) |
| [n]4180.5(2) | 85(4) |
| 4288.2(4) | 15(3) |
| 4432.3(2) | 30(2) |
| 4483.8(2) | 64(4) |
| 4577.3(2) | 54(3) |
| 4779.7(2) | 26(2) |
| 5010.70(2) | 106(4) |
| 5027.7(3) | 48(3) |
| 5133.6(3) | 51(3) |
| 5539.2(3) | 41(12) |
| 5674.7(6) | 31(3) |
| 5738.1(4) | 37(13) |
| [n]5900.1(6) | 26(10) |
| 5923(1) | 25(8) |
| 6109.3(5) | 24(8) |
| [n]6148.0(4) | 58(4) |
| 6207.4(5) | 36(3) |
| 6339.0(3) | 75(4) |
| 6376.4(4) | 39(3) |
| [n]6620(1) | [14(3)] |
| 6766.5(4) | 79(7) |
| 6822(2) | [15(12)] |
| 6977.1(2) | [31(23)] |
| 7073.3(3) | [23(18)] |
| 7168.8(5) | 102(6) |
| 7407.1(6) | 45(4) |
| 7587.0(5) | 53(17) |
| 7772(2) | 41(14) |
| 7893.1(6) | 50(5) |
| 7945(1) | 141(9) |

[a]The notation 110.370(2) is equivalent to $110.370 \pm 0.002$.
[n]Not listed in Refs. [12,26].

components, the contribution due to the radioactivity of the sample was strongly reduced by the very low duty factor of the n_TOF facility, while the effect of sample scattered neutrons was relaxed by the minimized neutron sensitivity of the detector system, in spite of the unfavorable scattering to capture detection efficiency ratio of $^{93}$Zr.

## IV. MAXWELLIAN-AVERAGED CROSS SECTIONS

The Maxwellian-averaged capture cross sections (MACS) are required for a quantitative description of the $s$ abundances produced during different phases of stellar evolution [4]. MACS can be calculated by folding the capture cross section with the respective thermal neutron spectrum at the $s$-process site. To cover all possible scenarios, cross-section data should be available over a sufficiently wide neutron energy range, starting at about 100 eV and extending to about 500 keV to account for the highest temperatures reached during shell carbon burning in massive stars.

TABLE III. Resonance parameters of the stable Zr isotopes extracted from the present data compared to results obtained with enriched samples [27–31]. All registered differences are inside experimental uncertainties.

| Isotope | $E_R$ (eV) | $K \pm \Delta K$ (meV) Enriched sample | $K \pm \Delta K$ (meV) Present data | Difference (%) |
|---|---|---|---|---|
| $^{90}$Zr | 3861 | 77 ± 2 | 79 ± 8 | 2.6 |
| $^{90}$Zr | 4008 | 130 ± 5 | 123 ± 10 | 5.4 |
| $^{91}$Zr | 159.5 | 0.0924 ± 0.0034 | 0.10 ± 0.01 | 8.7 |
| $^{91}$Zr | 182.0 | 4.99 ± 0.02 | 5.0 ± 0.3 | 0.2 |
| $^{91}$Zr | 240.4 | 1.61 ± 0.02 | 1.73 ± 0.12 | 7.5 |
| $^{91}$Zr | 292.7 | 58.9 ± 0.2 | 58 ± 2 | 1.6 |
| $^{91}$Zr | 449.8 | 2.03 ± 0.08 | 2.0 ± 0.1 | 1.5 |
| $^{92}$Zr | 2013 | 44.3 ± 1.1 | 44 ± 3 | 0.7 |
| $^{92}$Zr | 2689 | 115 ± 2 | 121 ± 6 | 5.2 |
| $^{92}$Zr | 4640 | 100 ± 3 | 106 ± 9 | 6.0 |
| $^{92}$Zr | 5046 | 142 ± 3 | 145 ± 9 | 2.1 |
| $^{94}$Zr | 2241 | 66.5 ± 1. | 68 ± 4 | 2.3 |
| $^{94}$Zr | 4925 | 126 ± 5 | 126 ± 7 | 0.0 |
| $^{96}$Zr | 301 | 113.3 ± 0.3 | 115 ± 3 | 1.5 |
| $^{96}$Zr | 3821 | 35 ± 1 | 33 ± 3 | 5.7 |
| $^{96}$Zr | 4135 | 106 ± 3 | 108 ± 30 | 1.9 |

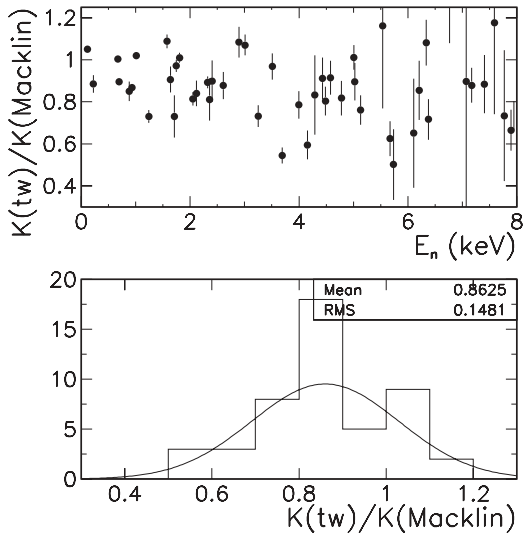


FIG. 3. Top: Ratio between capture kernels obtained in this work (tw) and those given by Macklin *et al.* [12]. Bottom: Distribution of kernel ratios.

Given the restricted energy range of this work, the present results have to be complemented for the neutron energy range above 8 keV, for instance, with evaluation data from cross-section libraries [32,33]. The impact of the present work has been estimated by means of a comparison with the $^{93}$Zr cross section of the recently released JENDL-4.0 library [33].

The contribution of the present results to the MACS values is illustrated for different thermal energies in the upper panel of Fig. 4, which shows the fraction of the MACS that is obtained if the integration is limited to neutron energies below 8 keV relative to the total MACS. One finds that already for the relevant value of $kT = 8$ keV only 50% of the MACS is contributed by the region below 8 keV neutron energy.

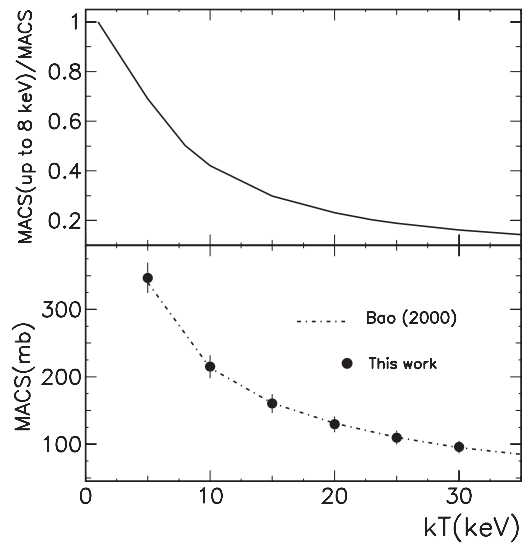


FIG. 4. Top: Ratio between MACS values calculated with an upper integration limit of 8 keV and the total MACS obtained by complementing the experimental results by evaluated data in Ref. [33]. Bottom: MACS as a function of thermal energy.

TABLE IV. MACS values (in mb) at different thermal energies.

| Thermal energy (keV) | $E_n \leqslant 8$ keV | | Full range | |
|---|---|---|---|---|
| | Ref. [33] | This work | Ref. [33] | This work[a] |
| 5 | 250 | 246 ± 12 | 354 | 347 ± 19 |
| 10 | 99 | 95 ± 5 | 223 | 215 ± 17 |
| 15 | 52 | 50 ± 3 | 166 | 160 ± 14 |
| 20 | 32 | 30 ± 2 | 134 | 129 ± 12 |
| 25 | 22 | 20 ± 1 | 114 | 110 ± 10 |
| 30 | 16 | 15 ± 1 | 99 | 96 ± 9 |

[a]Present results complemented above 8 keV by JENDL-4.0 data, renormalized by 0.97.

The partial contributions to the MACS from the energy range below 8 keV are compared in columns two and three of Table IV, showing that the entries based on this work are in fair agreement with those obtained with the JENDL data [33]. In spite of the new resonances, the present results are lower by 2–4% due to the slightly smaller capture kernels.

Accordingly, the JENDL data [33] were scaled by a factor 0.97 to match the present results before being used in the determination of the final MACS values. The associated uncertainties are composed of the 5% uncertainty of the present data and a 10% contribution ascribed to the evaluated data above 8 keV. In this way, the MACS value at $kT = 30$ keV is found in excellent agreement with the recommended value of $95 \pm 10$ mb [34], which is based on the results of Ref. [12]. However, it must be considered that if resonances at neutron energies higher than 8 keV were missed and/or mistakenly assigned in the past analysis [12], MACS values could displace from the recommended value [34]. In this sense, accurate future measurements at higher neutron energies are needed.

## V. CONCLUSIONS

The neutron capture reaction of $^{93}$Zr has been measured with improved accuracy in the neutron energy range up to 8 keV at the CERN n_TOF facility. In total, 64 resonances have been assigned to $^{93}$Zr. Nine of these have not been reported before. The high resolution of present measurement and of those performed at n_TOF on the other stable zirconium isotopes allowed in some cases for a correct nucleus-resonance assignment. Resonance parameters have been extracted by means of the $\mathcal{R}$-matrix code SAMMY. On average, the respective capture kernels have been found 14% smaller than reported previously. In the calculation of Maxwellian averaged cross sections the smaller capture kernels are balanced by the contribution of newly found resonances, resulting in very good agreement with past results. Given that the agreement comes from a mix of opposite weighting factors, new measurements at higher incident neutron energies are necessary to confirm the present results.

## ACKNOWLEDGMENTS

This work was supported by the EC under contract FIKW-CT-2000-00107 and by the funding agencies of the participating institutes.

[1] G. Wallerstein *et al.*, Rev. Mod. Phys. **69**, 995 (1997).
[2] E. M. Burbidge, G. R. Burbidge, W. A. Fowler, and F. Hoyle, Rev. Mod. Phys. **29**, 547 (1957).
[3] P. Seeger, W. Fowler, and D. Clayton, Ap. J. Suppl. **97**, 121 (1965).
[4] R. Gallino, C. Arlandini, M. Busso, M. Lugaro, C. Travaglio, O. Straniero, A. Chieffi, and M. Limongi, Astrophys. J. **497**, 388 (1998).
[5] C. M. Raiteri, M. Busso, R. Gallino, and G. Picchio, Astrophys. J. **371**, 665 (1991).
[6] T. Bernatowicz, G. Fraundorf, T. Ming, E. Anders, B. Wopenka, E. Zinner, and P. Fraundorf, Nature **330**, 728 (1987).
[7] M. Lugaro, *Stardust from Meteorites. An Introduction to Presolar Grains (Stardust from Meteorites)*, World Scientific Series in Astronomy and Astrophysics, Vol. 9 (World Scientific, Singapore, 2005).
[8] M. Lugaro, A. M. Davis, R. Gallino, M. J. Pellin, O. Straniero, and F. Käppeler, Astrophys. J. **593**, 486 (2003).
[9] Y. Kashiv, A. M. Davis, R. Gallino, Z. Cai, B. Lai, S. R. Sutton, and R. N. Clayton, Astrophys. J. **713**, 212 (2010).
[10] D. L. Lambert, V. V. Smith, M. Busso, R. Gallino, and O. Straniero, Astrophys. J. **450**, 302 (1995).
[11] A. Takibaev, M. Saito, V. Artisyuk, V. Apse, and A. Shmelev, J. Nucl. Sci. Technol. **37**, 870 (2000).
[12] R. L. Macklin, Astrophys. Space Sci. **115**, 71 (1985); R. L. Macklin, J. A. Harvey, and N. W. Hill, Nucl. Sci. Eng. **92**, 525 (1986).
[13] S. Nakamura, H. Harada, S. Raman, and P. E. Koehler, J. Nucl. Sci. Technol. **44**, 21 (2007).
[14] C. Borcea *et al.*, Nucl. Instr. Meth. A **513**, 523 (2003).
[15] U. Abbondanno *et al.*, CERN n_TOF Facility: Performance Report, CERN-SL-2002-053 ECT, 2003 (unpublished).
[16] S. Marrone *et al.*, Nucl. Instr. Meth. A **517**, 389 (2004).
[17] R. Plag *et al.*, Nucl. Instr. Meth. A **496**, 425 (2003).
[18] U. Abbondanno *et al.*, Nucl. Instr. Meth. A **538**, 692 (2005).
[19] F. Corvi *et al.*, Nucl. Sci. Eng. **107**, 272 (1991).
[20] J. N. Wilson *et al.*, Nucl. Instr. Meth. A **511**, 388 (2003).
[21] U. Abbondanno *et al.*, Nucl. Instr. Meth. A **521**, 454 (2004).
[22] R. Terlizzi *et al.*, Phys. Rev. C **75**, 035807 (2007).
[23] R. L. Macklin and J. Halperin, Phys. Rev. C **14**, 1389 (1976).
[24] N. M. Larson, Report ORNL/TM-9179/R7, Oak Ridge National Laboratory, 2006 (unpublished).
[25] J. E. Lynn, *Theory of Neutron Resonance Reactions* (Clarendon, Oxford, 1968); E. R. Rae *et al.*, Nucl. Phys. **5**, 89 (1958).
[26] S. F. Mughabghab, *Atlas of Neutron Resonances, Resonance Parameters and Thermal Cross Sections* $Z=1$–$100$ (Elsevier Science, Amsterdam, 2006).
[27] G. Tagliente *et al.*, Phys. Rev. C **77**, 035802 (2008).
[28] G. Tagliente *et al.*, Phys. Rev. C **78**, 045804 (2008).
[29] G. Tagliente *et al.*, Phys. Rev. C **81**, 055801 (2010).
[30] G. Tagliente *et al.*, Phys. Rev. C **84**, 015801 (2011).
[31] G. Tagliente *et al.*, Phys. Rev. C **84**, 055802 (2011).
[32] M. B. Chadwick, P. Oblozinsky, M. Herman *et al.*, Nucl. Data Sheets **107**, 2931 (2006).
[33] K. Shibata *et al.*, J. Nucl. Sci. Technol. **48**, 1 (2011).
[34] Z. Y. Bao, H. Beer, F. Käppeler, F. Voss, K. Wisshak, and T. Rauscher, At. Data Nucl. Data Tables **76**, 70 (2000).